Environmental Science & Technology

pubs.acs.org/est

Article

Improving the Thermodynamic Energy Efficiency of Battery Electrode Deionization Using Flow-Through Electrodes

Moon Son, Vineeth Pothanamkandathil, Wulin Yang, Johannes S. Vrouwenvelder, Christopher A. Gorski, and Bruce E. Logan*

Cite This: *Environ. Sci. Technol.* 2020, 54, 3628−3635

Read Online

ACCESS | Metrics & More | Article Recommendations | Supporting Information

ABSTRACT: Ion intercalation electrodes are being investigated for use in mixed capacitive deionization (CDI) and battery electrode deionization (BDI) systems because they can achieve selective ion removal and low energy deionization. To improve the thermodynamic energy efficiency (TEE) of these systems, flow-through electrodes were developed by coating porous carbon felt electrodes with a copper hexacyanoferrate composite mixture. The TEE for ion separation using flow-through electrodes was compared to a system using flow-by electrodes with the same materials. The flow-through BDI system increased the recoverable energy nearly 3-fold (0.009 kWh m^{-3}, compared to a 0.003 kWh m^{-3}), which increased the TEE from ∼6% to 8% (NaCl concentration reduction from 50 to 42 mM; 10 A m^{-2}, 50% water recovery, and 0.5 mL min^{-1}). The TEE was further increased to 12% by decreasing the flow rate from 0.50 to 0.25 mL min^{-1}. These findings suggest that, under similar operational conditions and materials, flow-through battery electrodes could achieve better energy recovery and TEE for desalination than flow-by electrodes.

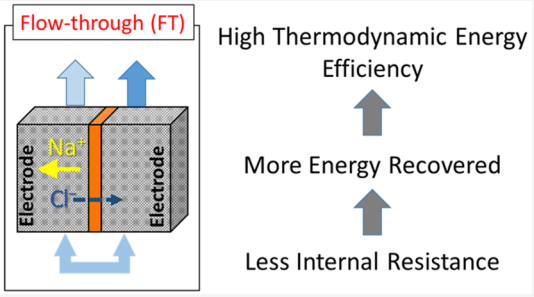

INTRODUCTION

Several different electrochemical processes, including capacitive deionization (CDI), electrodialysis, shock electrodialysis, and electro-forward osmosis, are being investigated as methods to achieve more efficient deionization of brackish waters.[1−8] CDI has been widely investigated because of its use of inexpensive electrode materials, such as activated carbon, and relatively low energy requirements (<0.5 kWh m^{-3} for <25 mM NaCl).[9−15] A typical CDI cell consists of two capacitive electrodes that remove ions via an electrostatic double layer when current is applied. The ions held by the electrodes in the first charging step are released in a second discharging step by alternating the direction of the applied current. One disadvantage of CDI is that high applied voltages (>1.2 V) can result in parasitic Faradaic reactions, such as hydrogen evolution at the cathode or anode oxidation.[16,17]

A slightly different approach to electrochemical desalination is based on one or both of the capacitive electrodes being replaced by battery-type or intercalation materials, such as Prussian Blue or manganese oxides.[18−21] This process, called Faradaic deionization,[22] cation intercalation desalination,[23] or battery electrode deionization (BDI),[19,24] can reduce the energy used for desalination compared to CDI as specific voltages are used to intercalate the ions into the electrode material, rather than hold them on the electrode surface. In recent BDI tests using the Prussian Blue analogue copper hexacyanoferrate (CuHCF),[19] efficient desalination was achieved at an applied voltage of 0.6 V, with 0.02 kWh m^{-3} for a triple stack of ion exchange membranes, and 0.05 kWh m^{-3} for a single membrane (25 mM NaCl influent and 17 mM effluent). In contrast, ∼0.2 kWh m^{-3} was required using CDI under the same experimental conditions.[19] One goal for improving the efficiency of the BDI process is to increase the thermodynamic energy efficiency (TEE) of the system, where TEE is defined as the amount of energy used by an actual system relative to the thermodynamic minimum energy required to achieve a particular salt separation.[25]

To improve the overall efficiency of the BDI system, we examined the use of flow-through electrodes constructed by depositing a composite mixture of CuHCF, binder, and carbon black into a highly porous graphite felt substrate. The complete cell consisted of two flow-through CuHCF electrodes in direct contact with an anion exchange membrane (AEM) placed in the middle of the chamber. This configuration is slightly different from a flow-through CDI process, where an AEM is not usually used, and where the feed stream flows perpendicular to the electrodes.[26] In the flow-through BDI system, the feed stream penetrates the electrode in a direction parallel to the water flow. Sodium ions are intercalated into the

Received: November 12, 2019
Revised: January 28, 2020
Accepted: February 24, 2020
Published: February 24, 2020

https://dx.doi.org/10.1021/acs.est.9b06843
Environ. Sci. Technol. 2020, 54, 3628−3635

positive electrode while chloride ions migrate through the AEM toward the counter electrode. A semicontinuous treatment process is created by switching the direction of the applied voltage (0.6 V). While there have been several flow-through CDI systems,[27−30] there is only one previously reported flow-through electrode system in deionization using cation intercalation electrodes.[23] However, that study did not provide comparisons with flow-by electrodes with the same architecture. Thus, one of the objectives of this study was to compare TEE values recorded for BDI systems using flow-through or flow-by electrodes with the same general architecture. In typical CDI systems that use porous carbon electrodes, a higher average salt adsorption rate was observed in the flow-through mode compared to the flow-by mode because of the longer electrode−solution contact time.[26,31] However, this increased adsorption rate results in a decreased TEE in the flow-through mode due to the additional resistance of the separator in between two electrodes and increased rates of faradaic side reactions.[13,32,33] Unlike a CDI system, the BDI system does not have a separator in the water path, and it operates at relatively low voltage, which could increase TEE values. To more fully evaluate the impact of the flow-through configuration, we compared flow-through BDI electrodes with a flow-by configuration used in our previous studies.[19] To further improve performance, the flow-through configuration was also examined with higher CuHCF loading. The performance of these systems was evaluated in terms of specific adsorption capacity of Na^+ ions, specific capacity of charge, charge efficiency, cycling efficiency, energy consumption, energy recovery, and TEE.

MATERIALS AND METHODS

Battery Electrode Fabrication. CuHCF powder was synthesized using a coprecipitation method as previously reported.[19,24] Briefly, the same amounts of 0.1 M $Cu(NO_3)_2$ (Sigma-Aldrich) and 0.05 M $K_3[Fe(CN)_6]$ (J.T. Baker) were added to deionized (DI) water with vigorous stirring. The precipitates were washed by centrifugation and dried overnight in a vacuum oven to produce the CuHCF powder. A slurry of CuHCF (80 wt %), carbon black (10 wt %, Vulcan XC72R, Cabot, average particle size = 50 nm), and polyvinyledene-fluoride (10 wt %, Kynar HSV 900, Arkema Inc.) in 1-methyl-2-pyrrolidinone (Sigma-Aldrich) was loaded onto the substrate using a pipet to fabricate electrodes containing 5 mg cm^{-2} of the slurry (4 mg cm^{-2} of CuHCF). A graphite felt substrate (3.0 mm thick and ∼31 mg cm^{-2}; CeTech, GF030) was used to make the flow-through (FT) electrodes, while carbon cloth (0.25 mm thick and ∼20 mg cm^{-2}; AvCarb Material Solutions, 1071 HCB) was used for the control experiments with flow-by (FB) electrodes. Preliminary tests showed that it was possible approximately double the amount of CuHCF slurry added to the felt electrodes; further addition of the slurry clogged the electrode so that no flow could be passed through the electrode. For the double-loaded electrodes, 10 mg cm^{-2} of the slurry containing 8 mg cm^{-2} of CuHCF was loaded onto carbon cloth (FB-D) or graphite felt substrates (FT-D). All the electrodes were heated and dried at 70 °C using a vacuum oven to remove the solvent.

Electrode Characterization. Scanning electron microscopy (SEM, Apreo, ThermoFisher Scientific) and energy dispersive X-ray spectroscopy (EDS) were used to determine the morphology and dispersion of CuHCF powder in the electrodes. Standard and backscatter detectors were used to ensure a distinction between CuHCF powder and carbon-based substrates. No separate conductive coating of the samples was conducted since the electrode itself was highly conductive.

The electrode porosity (P, %), was calculated using[34]

$$P = \frac{W_w - W_d}{E_a h} \times 100 \quad (1)$$

where W_w (g) is the weight of the electrode after it filled with water by pulling water into it using a vacuum pump, W_d (g) is the dry electrode weight (g), E_a (cm^2) is the electrode surface area, and h (cm) is the electrode thickness.

Cyclic voltammetry (CV) of each electrode was measured using a 3-electrode cell (∼2 cm long by ∼3 cm in diameter) containing working and counter CuHCF electrodes, and a Ag/AgCl reference electrode, at a scan rate of 1 mV s^{-1} using 1 M NaCl.

BDI Cell Construction. The BDI cell of cylindrical chambers (30 mm exposed diameter, 7 cm^2 effective area) containing two CuHCF electrodes separated by an AEM (106 ± 1 μm thick with an ion exchange capacity of 1.85 mmol g^{-1},[35,36] Selemion AMV, Asahi Glass) (Figure 1). For both FT and FB operation, the water entered the bottom of the chamber and exited through the top of each chamber. In FT mode, the water flowed through the electrode that completely filled the chamber (no spacer), with flow into the other chamber blocked by the AEM. In FB mode, the same configuration was used except the water flowed through over the electrode through a fabric spacer (0.28 mm thick and 33% porosity; Sefar Nitex, 06-210/33). Rubber gaskets were placed between each component to prevent leakage of solution and graphite foil was used as the current collector for the CuHCF electrodes. Conductivity of the effluent solutions was monitored using a flow-through conductivity meter (ET908, eDAQ, Australia). Prior to desalination tests, the potentials of the two CuHCF electrodes were adjusted to 0.4 and 1.0 V (versus Ag/AgCl reference electrodes) using a separate 3-electrode cell containing working (CuHCF), counter (activated carbon), reference electrodes (Ag/AgCl in 3 M NaCl), and 1 M NaCl solution, as previously described.[19]

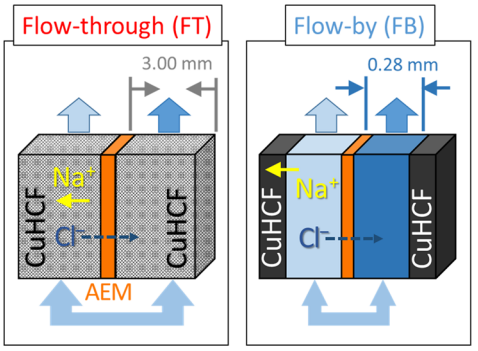

Figure 1. Schematic of flow-through (FT) and flow-by (FB) deionization cells using battery electrodes composed of copper hexacyanoferrate (CuHCF) in two channels divided by an anion exchange membrane (AEM).

Desalination Experiments. Electrochemical removal of sodium ions by the CuHCF can be expressed as

https://dx.doi.org/10.1021/acs.est.9b06843
Environ. Sci. Technol. 2020, 54, 3628−3635

$$Na^+Cu[Fe^{III}(CN)_6] + xNa^+ + xe^- = Na^+_{1+x}Cu[Fe^{II}(CN)_6]_x[Fe^{III}(CN)_6]_{1-x} \quad (2)$$

where Na^+ stands for sodium ion present in the feed solution. The CuHCF electrode can hold sodium (3.6 Å hydrated radius) or other ions when they are similar in size to the interstitial sites (3.2~4.6 Å).[37−41] Synthetic brackish water (50 mM NaCl) was continuously fed to the BDI cell at a flow rate of 0.5 mL min^{-1}, except as noted. A set current of 10 A m^{-2} was applied at a voltage window of ±0.6 V using a potentiostat (VMP3, Bio-Logic), except as indicated. The NaCl concentrations in the effluent were reported based on the measured solution conductivities.

Specific adsorption capacity (SAC, mg of Na^+ per gram of electrode, mg g^{-1}) was calculated as

$$SAC = \frac{M_{Na}\int_0^{T_c} C_{Na}\, dt}{E_{mass}} \quad (3)$$

where T_c is the charging time or the cycling time, C_{Na} is the moles of Na^+ removed, M_{Na} is the molecular weight of Na^+, and E_{mass} is the electrode mass. Specific capacity (SC, mAh g^{-1}) was calculated as

$$SC = \frac{\int_0^{T_c} I\, dt}{E_{mass}} \quad (4)$$

where I is the applied current. Charge efficiency (Λ; %) was calculated as

$$\Lambda = \frac{F\int_0^{T_c} C_{Na}\, dt}{\int_0^{T_c} I\, dt} \times 100 \quad (5)$$

where F is Faraday's constant (96 485 C mol^{-1}). Cycling efficiency (CE; %) was calculated as

$$CE = \frac{\sum T_D}{\sum T_C} \times 100 \quad (6)$$

where T_D is the discharge time. The discharge and charge times are the time taken for the voltage to increase from −0.6 to 0.6 V or decrease from 0.6 to −0.6 V at a constant current, 10 A m^{-2}.

Thermodynamic Energy Efficiency. Energy consumption (E_C, kWh m^{-3}) and recovery (E_R, kWh m^{-3}) were calculated as[19]

$$E_C = \frac{\int_0^{T_s} VI\, dt}{J_w} \quad (7)$$

$$E_R = \frac{\int_0^{T_f} VI\, dt}{J_w} \quad (8)$$

where T_f is the beginning of the first half-cycle when the flows are switched (−0.6 to 0 V when 10 A m^{-2} is applied or 0.6 to 0 V when −10 A m^{-2} is applied), T_s is the rest of the half-cycle until the direction of applying current is switched, and J_w is the water flux during operation (during T_f and T_s). During the ion adsorption step (T_s), the voltage (V) and the current (I) have the same sign (either positive or negative), meaning that this step costs energy. However, during the ion desorption step (T_f), the voltage (V) and the current (I) have the different signs since ions are released spontaneously, so that this step recovers energy. Thus, energy recovery was calculated when the direction of the applied current is switched until the cell voltage reached 0 V (Figure S1).

The thermodynamic energy efficiency (TEE, %) was calculated as

$$TEE = \frac{\Delta g}{E_C - E_R} \times 100 \quad (9)$$

The specific Gibbs free energy of separation, Δg (kWh m^{-3}), was calculated as[42]

$$\Delta g = 2RT_a\left\{\frac{C_0}{\gamma}\ln\left[\frac{C_0 - \gamma C_D}{C_0(1-\gamma)}\right] - C_D\ln\left[\frac{C_0 - \gamma C_D}{C_D(1-\gamma)}\right]\right\} \quad (10)$$

where R is the ideal gas constant, T_a is the absolute temperature, C_0 is the feed concentration, C_D is the stabilized product water concentration, and γ is the water recovery. In all experiments, the flow rate of both chambers remained the same, so the water recovery was fixed at 50% (γ = 0.5).

RESULTS AND DISCUSSION

Flow-through vs Flow-By Battery Electrode Performance. The FT battery electrode could be operated for a longer period of time (18 vs 14 min for the FB electrode) before ion saturation occurred, resulting in a slower increase in cell voltage compared to that obtained with the FB electrode for a complete charging/discharging cycle (constant current of 10 A m^{-2}, voltage window of ±0.6 V) (Figure 2). This longer operation time of the FT electrode can be explained by the lower ohmic (or IR) drop. When the direction of the current is changed under constant current conditions, the voltage of the electrode instantaneously decreases due to the internal resistance of the cell.[43] The magnitude of the change in the voltage change reflects the internal resistance of a cell, and

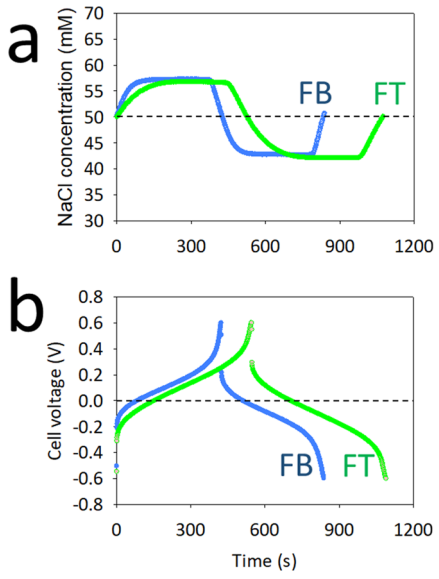

Figure 2. (a) Representative effluent concentration profiles and (b) cell voltages of the FT and FB electrodes for one complete cycle. A constant current of 10 A m^{-2} was applied at a voltage window of ±0.6 V.

https://dx.doi.org/10.1021/acs.est.9b06843
Environ. Sci. Technol. 2020, 54, 3628−3635

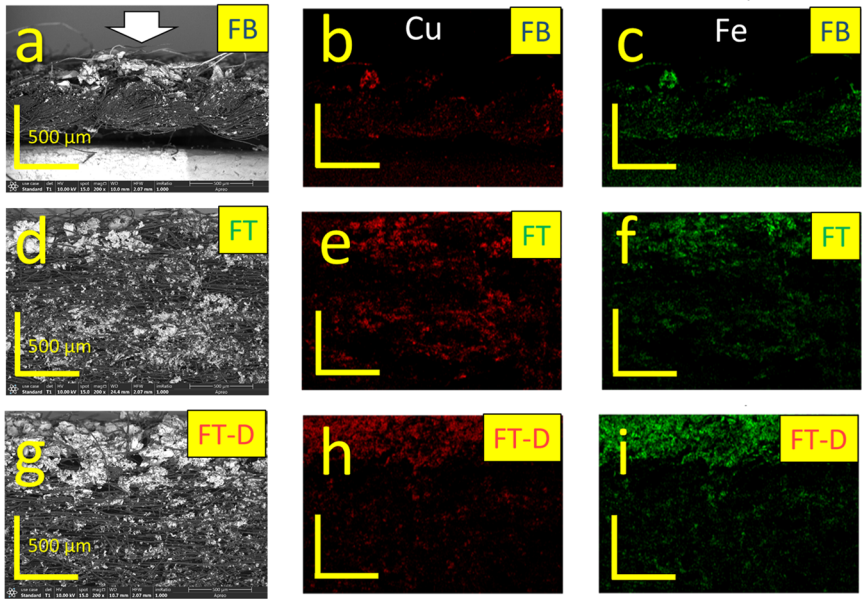

Figure 3. Cross-sectional images of the FB, FT, and FT-D (FT electrode with double CuHCF loading) electrodes using (a, d, and g) SEM and (b, e, and h) Cu and (c, f, and i) Fe using SEM-EDS. The white arrow indicates the direction the slurry containing CuHCF was deposited. Scale bars (yellow) are 500 μm in both horizontal (x) and vertical (y) directions.

therefore the smaller voltage drop for the FT electrode (0.3 V in 2 s) shows that it had a lower internal resistance than the FB electrode (0.4 V in 2 s). This lower internal resistance was due to better dispersion of CuHCF, a longer retention time of the feed solution, and less solution resistance due to the lack of a gap between the electrode and AEM in the FT configuration compared to the FB configuration. Since both FT and FB electrodes were tested in essentially the same flow-cell architecture with the same electrode material, the influence of other factors that determine overall resistance in the electrochemical processes can be excluded in our comparisons, such as contact resistances at current collectors and collector resistance.[32]

Although the same amount of the CuHCF (4 mg cm^{-2}) was used for both the FT and FB electrodes, the electrode material was better dispersed throughout the FT electrode compared to FB electrode (Figures 3 and S2). This better dispersion of the CuHCF within the electrode provided more active sites, contributing to the lower ohmic drop for the FT electrode. The longer retention time of the fluid is also known from previous studies to help reduce the ohmic drop.[9] On the basis of the thickness and porosity of the porous substrate (3.00 mm and 89 ± 4%) and spacer (0.28 mm and 33%), the hydraulic retention time (HRT) of FT cell (3.74 min) was 28 times greater than FB cell (0.13 min). This longer HRT can also explain the slightly slower salt adsorption kinetics of the FT electrode compared to the FB electrode when the current was switched. As a result of the larger HRT of the FT cells, the NaCl concentration of the effluent solution reached a plateau more slowly when the voltage was applied compared to the FB cell (Figure 2a). Thus, the lower internal resistance of the FT cell was most likely from its better dispersion of CuHCF, longer HRT, and less solution resistance since the chemical composition of the electrode itself (CuHCF and carbon-based substrate) was not changed.

The FT electrode had a higher specific capacity (SC = 35 mAh g^{-1}) and salt adsorption capacity (SAC = 19 mg-Na g^{-1}) than the FB electrode (SC = 29 mAh g^{-1}, SAC = 17 mg-Na g^{-1}). These larger values for the FT electrode, with the same CuHCF loading, was likely due to the greater availability of active sites since both the FT and FB electrodes had the same total capacitance, as shown in the CV profiles (Figure 4). This

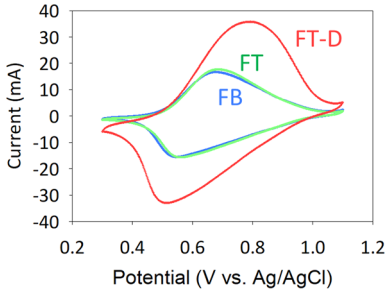

Figure 4. Representative cyclic voltammetry (CV) scans of FB (blue line), FT (green line), and FT-D (red line) electrodes in a 3-electrode cell (1 M NaCl, scan rate = 1 mV s^{-1}). The FB and FT lines overlap each other and, thus, are difficult to distinguish.

improved performance for the FT electrode is consistent with previous findings that using three-dimensional electrodes improves electrode performances due to a large surface area and greater charge transport.[44] The cycling efficiencies of the two battery electrodes was both very high (100% for FT; 99% for FB), indicating nearly identical times for charging and discharging for each electrode.

An additional experiment was conducted with a plain carbon electrode, typically used for CDI, in order to confirm that ion adsorption was not affected by the electrode capacitance. When a plain carbon cloth electrode (4 mg cm^{-2} of activated-carbon, no CuHCF) was used, no appreciable change in the effluent solution was found under the same experiment conditions as that tested for the BDI electrodes (10 A m^{-2} and ±0.6 V) (Figure S3). Therefore, sodium ions were removed through intercalation in the presence of CuHCF and

https://dx.doi.org/10.1021/acs.est.9b06843
Environ. Sci. Technol. 2020, 54, 3628−3635

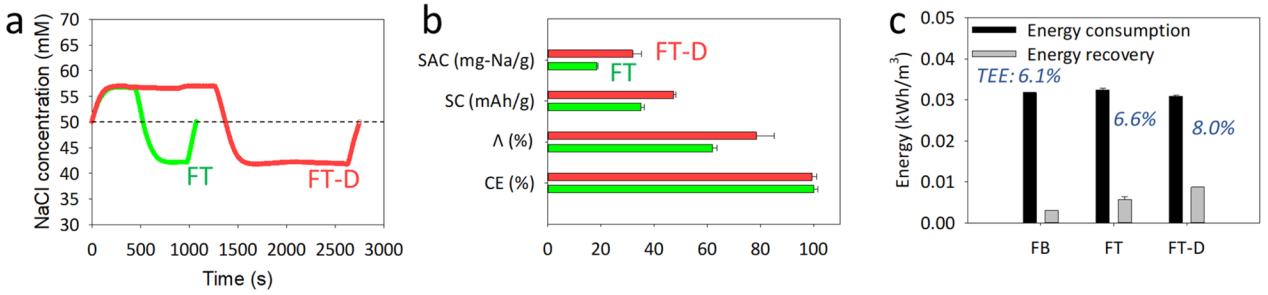

Figure 5. (a) Representative effluent concentration profiles of FT and FT-D (FT electrode with double loading of CuHCF) electrodes. (b) Specific adsorption capacity (SAC), specific capacity (SC), charge efficiency (Λ), and cycling efficiency (CE) of the electrodes. (c) Energy consumption and recovery and thermodynamic energy efficiency (TEE) of the electrodes. A constant current of 10 A m^{-2} was applied at a voltage window of ±0.6 V. Error bars show the range from at least duplicated experiments.

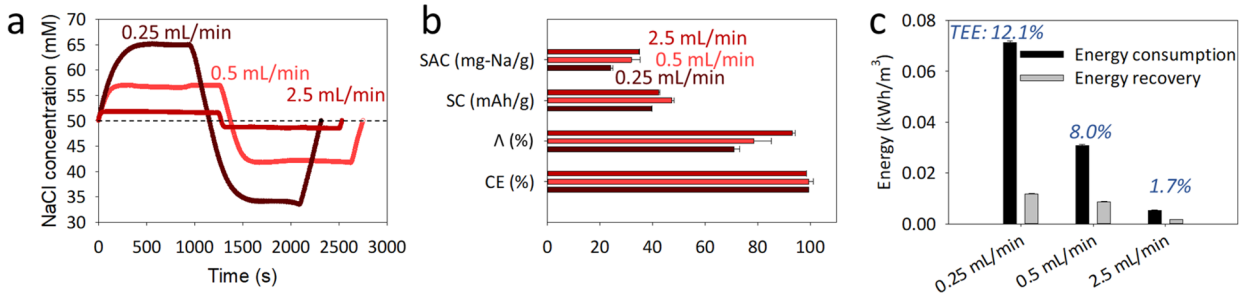

Figure 6. (a) Representative effluent concentration profiles as a function of flow rate, 0.25, 0.5, and 2.5 mL min^{-1}, using FT-D electrodes. (b) Specific adsorption capacity (SAC), specific capacity (SC), charge efficiency (Λ), and cycling efficiency (CE) at different flow rates. (c) Energy consumption and recovery and thermodynamic energy efficiency (TEE) at different flow rates. A set current of 10 A m^{-2} was applied at a voltage window of ±0.6 V. Error bars show the range from at least duplicated experiments.

not double layer adsorption by the capacitance of the electrode.

Effect of Adding More CuHCF. Additional CuHCF was added to the graphite felt, with a maximum amount limited to 8 mg cm^{-2} of CuHCF, or double that used in the previous experiments. The FT-D electrode operation time was almost three times longer than that of the FT electrode (Figure 5a), enabling three times more desalinated water to be produced per half-cycle of operation. The FT-D electrode also had considerably greater salt adsorption (SAC = 32 mg-Na g^{-1}) and specific (SC = 47 mAh g^{-1}) capacities, and a larger charge efficiency (Λ = 78%) than the FT electrodes (Figure 5b). Although the FT-D electrode had a higher capacitance than the FT electrode (Figure 4), the improved performance was mostly due to the greater mass of CuHCF, as shown by the nearly doubled salt adsorption capacity of the FT-D electrode. The CuHCF was better distributed into the whole felt FT-D electrode, compared to tests with less material (Figure 3g–i). This better CuHCF dispersion of the FT-D electrode along the substrate depth was clearly shown in the wide cross-sectional SEM image (Figure S2). The dispersion of the CuHCF was important because higher desalination performances would not have been achieved with more CuHCF mass loading if it was not well dispersed. The cycling efficiency of the FT-D electrode remained very high (CE = 99%), indicating the time to charge the electrode was the same as that needed to discharge the electrode. This double loading of CuHCF could not be successfully used for the cloth electrode for the FB tests. When this amount of material was added to the FB electrode, the deposited material had an uneven surface (Figure S4c), and preliminary tests showed reduced performance (data not shown).

The FT-D electrode had an increased TEE of 8.0% as a result of having three times greater energy recovery (0.009 kWh m^{-3}) than the FB electrode (0.003 kWh m^{-3}) (Figure 5c). Although both electrodes consumed the same total amount of energy (~0.03 kWh m^{-3}) to desalinate the solution (50 mM to 42 mM), the total time measured during the energy recovery step using the FT-D electrode was almost 8 times longer (~8 min) compared to that of the FB electrode (~1 min). This additional time was due to the lower internal resistance, and not differences in hydraulic retention times in the chamber, based on comparisons of the ohmic drop after the cutoff voltage was reached. The ohmic drop was 0.2 V for the FT-D electrode, compared to 0.3 V for the FT electrode, and 0.4 V for the FB electrode (Figure S5). The energy recovery of the FT-D electrode was also increased due to the slower rate of the voltage change of the FT-D electrode during the overall energy recovery step than that of the FB electrode (Figure S5).

Effect of Flow Rate. The water feed was set at a faster (2.5 mL min^{-1}) and slower (0.25 mL min^{-1}) flow rate to examine the impact of flow rate relative to that used in the previous tests (0.5 mL min^{-1}) (Figure 6). Decreasing the flow rate to 0.25 mL min^{-1} increased salt removal producing an effluent salt concentration of 34 mM, while increasing it to 2.5 mL min^{-1} substantially decreased salt removal, producing an effluent salt concentration of 48.5 mM (Figure 6a). Therefore, the extent of desalination was inversely proportional to the flow rate. However, the salt adsorption capacity and charge efficiency both increased with flow rate, with a 44% increase in SAC to 35 mg-Na g^{-1} and a change in the Λ from 71% to 93% at the highest flow rate (Figure 6b). These increases in SAC and Λ were due to the increased total amount of moles of Na^+

https://dx.doi.org/10.1021/acs.est.9b06843
Environ. Sci. Technol. 2020, 54, 3628−3635

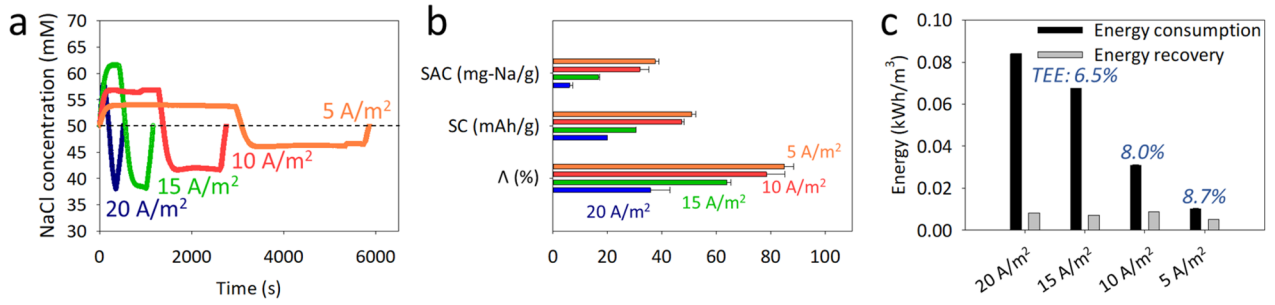

Figure 7. (a) Representative effluent concentration profiles as a function of constant current, 5, 10, 15, and 20 A m^{-2}, using FT-D electrodes. (b) Specific adsorption capacity (SAC), specific capacity (SC), and charge efficiency (Λ) at different constant currents. (c) Energy consumption and recovery and thermodynamic energy efficiency (TEE) at different constant currents. Error bars show the range from at least duplicated experiments.

ions removed at the higher flow rate, but a lower extent of ion removal relative to the 10 times higher flow rate into the cell.

The TEE increased to 12.1% by using the slower flow rate of 0.25 mL min^{-1}, due primarily to the greater extent of desalination (Figure 6c). At the slowest flow rate, the energy consumed was 0.071 kWh m^{-3}, compared to 0.005 kWh m^{-3} for the highest flow rate. Although the energy used by the highest flow rate was only 7% of that of the slowest flow rate, the energy for desalinating 50 mM influent water to 48.5 mL was <1% of the energy to obtain 34 mM effluent as a final concentration. This is in an excellent agreement with literature that the higher TEE can be obtained when the higher Gibbs free energy per volume of product water (~Δ*C*) was used.[33,45]

Effect of Current Density. The applied current density was increased (20 and 15 A m^{-2}) or decreased (5 A m^{-2}) to examine the impact of current density compared to that used in the previous tests (10 A m^{-2}) (Figure 7). The extent of desalination was highly dependent on the applied current density since the Na^+ removal rate is dependent on the current density. Thus, decreasing the current density produced lower effluent salt concentrations of 42 mM (10 A m^{-2}) and 46 mM (5 A m^{-2}) (Figure 7a). While increasing the current density to 15 A m^{-2} decreased the effluent salt concentration to 38.1 mM, but no further decrease in the effluent concentration was obtained at the highest applied current density of 20 A m^{-2}. At the two lowest current densities, the effluent concentration was stable for a period of time. However, at the two highest current densities, a very brief plateau (15 A m^{-2}) or only a maximum (20 A m^{-2}) with no plateau was observed for the effluent salt concentration (Figure 7a). This lack of a stable plateau indicated that the flux of Na^+ ions to the electrode was too low to maintain ion removal at current densities ≥15 A m^{-2} (Figure 7b). Thus, lower current densities are needed to maintain stable salt removals to obtain high SAC, SC, and Λ.

Decreasing the current density increased the specific adsorption capacity, specific capacity, and charge efficiency, indicating that ion removal was not limited by diffusion at the lower current densities (Figure 7b). For example, at the lowest current density (5 A m^{-2}), the specific adsorption capacity was more than 6 times higher (SAC = 37 mg-Na g^{-1}), and the charge efficiency more than 2 times higher (Λ = 85%) than those values obtained at 20 A m^{-2} (SAC = 6 mg-Na g^{-1}, Λ = 36%).

Lowering the current density decreased energy consumption (from 0.084 to 0.010 kWh m^{-3}), but energy recovery was less impacted (from 0.008 to 0.005 kWh m^{-3}) (Figure 7c). Thus, only 10% of energy was recovered when the current density of 20 A m^{-2} was used, while 51% of energy was recovered when 5 A m^{-2} was used. Therefore, the highest *TEE* of 8.7% was found at a current density of 5 A m^{-2}. Unlike the set of experiments by changing the flow rate (Figure 6), decreasing current density (Figure 7) exhibited an inverse correlation between the Gibbs free energy per volume of product water (~Δ*C*) and TEE due to the substantial decrease of charge efficiency at the high applied current density. On the basis of these changes in specific adsorption capacity, specific capacity, charge efficiency, and TEE with current density, operation at ≤10 A m^{-2} appeared to provide the best balance in overall system performance.

Outlook. The use of the FT type electrodes in the BDI increased water desalination performances (TEE of >8.0%) due a reduction in the ohmic drop. The improved TEE is in contrast with results reported in the CDI literature that FT electrodes are less energy-efficient due to the additional resistance of the separator and the increased rate of side reactions.[13,32,33] Unlike CDI systems, the absence of a separator in the water path, the use of a relatively low applied voltage, and the lower internal resistance in the BDI system all combine to increase TEE values from ~6% to 8%. The energy losses due to the higher pressures needed to force the liquid through the felt substrate were not included in this calculation. One way to reduce the energy needed to pump water through the electrode is to reduce the CuHCF particle size. The particles used here were ~200 μm in size (Figure S2), which could have clogged some of the pores in the felt. Therefore, it might be possible to reduce energy needed for pumping by loading load smaller particles onto the electrode fibers. However, flow through a porous bed of these particles alone, rather than primarily through the fibers, would increase pumping energy as the permeability changes inversely with particle size.

The optimal operation of the BDI systems depends on a number of factors, including flow rate, current density, and flow path. While lowering the flow rate improves the TEE, the extent of desalination is also reduced, offsetting this improvement. Increasing the current density also would further decrease the TEE. A more practical approach to improve energy efficiency would be to use 2−3 pairs of ion exchange membranes to desalinate additional water as previously shown.[19] Another issue that affects performance is the flow path through the electrode. The flow through the porous electrode used here may not be uniform, so a more channelized flow arrangement could improve performance. Ultimately, if a BDI system using an FT electrode can achieve a

https://dx.doi.org/10.1021/acs.est.9b06843
Environ. Sci. Technol. 2020, 54, 3628−3635

higher TEE over other processes in brackish water desalination, the electrochemical-based desalination system will have an advantage not only in terms of energy consumption but also due to an improved energy efficiency.

■ ASSOCIATED CONTENT

Supporting Information

The Supporting Information is available free of charge at https://pubs.acs.org/doi/10.1021/acs.est.9b06843.

Details on the effluent and cell voltage profiles recorded by using a FB electrode, the surface and cross-sectional SEM images of the FB, FT, and FT-D electrodes, the concentration profiles of NaCl effluent using activated carbon electrodes, the photographs of the electrodes, and the cell voltage profiles recorded by using the FB, FT, and FT-D electrodes during the energy recovery step (PDF)

■ AUTHOR INFORMATION

Corresponding Author

Bruce E. Logan − *Department of Civil and Environmental Engineering, The Pennsylvania State University, University Park, Pennsylvania 16802, United States;* orcid.org/0000-0001-7478-8070; Phone: +1-814-863-7908; Email: blogan@psu.edu; Fax: +1 814 863-7304

Authors

Moon Son − *Department of Civil and Environmental Engineering, The Pennsylvania State University, University Park, Pennsylvania 16802, United States;* orcid.org/0000-0002-3770-148X

Vineeth Pothanamkandathil − *Department of Civil and Environmental Engineering, The Pennsylvania State University, University Park, Pennsylvania 16802, United States*

Wulin Yang − *Department of Civil and Environmental Engineering, The Pennsylvania State University, University Park, Pennsylvania 16802, United States*

Johannes S. Vrouwenvelder − *Water Desalination and Reuse Center (WDRC), Division of Biological and Environmental Science and Engineering (BESE), King Abdullah University of Science and Technology (KAUST), Thuwal 23955-6900, Saudi Arabia*

Christopher A. Gorski − *Department of Civil and Environmental Engineering, The Pennsylvania State University, University Park, Pennsylvania 16802, United States;* orcid.org/0000-0002-5363-2904

Complete contact information is available at: https://pubs.acs.org/10.1021/acs.est.9b06843

Notes

The authors declare no competing financial interest.

■ ACKNOWLEDGMENTS

This research was supported by the King Abdullah University of Science and Technology (KAUST) (OSR-2017-CPF-2907-02) and Penn State University. Support for V.P. and C.A.G. was provided by the National Science Foundation under Grant 1749207.

■ REFERENCES

(1) Porada, S.; Zhao, R.; van der Wal, A.; Presser, V.; Biesheuvel, P. M. Review on the science and technology of water desalination by capacitive deionization. *Prog. Mater. Sci.* **2013**, *58* (8), 1388−1442.

(2) AlMarzooqi, F. A.; Al Ghaferi, A. A.; Saadat, I.; Hilal, N. Application of capacitive deionisation in water desalination: A review. *Desalination* **2014**, *342*, 3−15.

(3) Jeon, S.-i.; Park, H.-r.; Yeo, J.-g.; Yang, S.; Cho, C. H.; Han, M. H.; Kim, D. K. Desalination via a new membrane capacitive deionization process utilizing flow-electrodes. *Energy Environ. Sci.* **2013**, *6* (5), 1471−1475.

(4) Lee, J.; Kim, S.; Kim, C.; Yoon, J. Hybrid capacitive deionization to enhance the desalination performance of capacitive techniques. *Energy Environ. Sci.* **2014**, *7* (11), 3683−3689.

(5) Kim, Y.; Logan, B. E. Series assembly of microbial desalination cells containing stacked electrodialysis cells for partial or complete seawater desalination. *Environ. Sci. Technol.* **2011**, *45* (13), 5840−5845.

(6) Kim, Y.; Logan, B. E. Microbial reverse electrodialysis cells for synergistically enhanced power production. *Environ. Sci. Technol.* **2011**, *45* (13), 5834−5839.

(7) Schlumpberger, S.; Lu, N. B.; Suss, M. E.; Bazant, M. Z. Scalable and continuous water deionization by shock electrodialysis. *Environ. Sci. Technol. Lett.* **2015**, *2* (12), 367−372.

(8) Son, M.; Kim, T.; Yang, W.; Gorski, C. A.; Logan, B. E. Electro-forward osmosis. *Environ. Sci. Technol.* **2019**, *53* (14), 8352−8361.

(9) Zhao, R.; Porada, S.; Biesheuvel, P. M.; van der Wal, A. Energy consumption in membrane capacitive deionization for different water recoveries and flow rates, and comparison with reverse osmosis. *Desalination* **2013**, *330*, 35−41.

(10) Zhao, R.; Biesheuvel, P. M.; van der Wal, A. Energy consumption and constant current operation in membrane capacitive deionization. *Energy Environ. Sci.* **2012**, *5* (11), 9520−9527.

(11) Lee, J.-H.; Bae, W.-S.; Choi, J.-H. Electrode reactions and adsorption/desorption performance related to the applied potential in a capacitive deionization process. *Desalination* **2010**, *258* (1), 159−163.

(12) Farmer, J. C.; Fix, D. V.; Mack, G. V.; Pekala, R. W.; Poco, J. F. Capacitive deionization of NaCl and $NaNO_3$ solutions with carbon aerogel electrodes. *J. Electrochem. Soc.* **1996**, *143* (1), 159−169.

(13) Długołęcki, P.; van der Wal, A. Energy recovery in membrane capacitive deionization. *Environ. Sci. Technol.* **2013**, *47* (9), 4904−4910.

(14) Ahualli, S.; Iglesias, G. R.; Fernández, M. M.; Jiménez, M. L.; Delgado, Á. V. Use of soft electrodes in capacitive deionization of solutions. *Environ. Sci. Technol.* **2017**, *51* (9), 5326−5333.

(15) Zhao, R.; Biesheuvel, P.; Miedema, H.; Bruning, H.; Van der Wal, A. Charge efficiency: a functional tool to probe the double-layer structure inside of porous electrodes and application in the modeling of capacitive deionization. *J. Phys. Chem. Lett.* **2010**, *1* (1), 205−210.

(16) Zhang, C.; He, D.; Ma, J.; Tang, W.; Waite, T. D. Faradaic reactions in capacitive deionization (CDI) - problems and possibilities: A review. *Water Res.* **2018**, *128*, 314−330.

(17) Tang, W.; He, D.; Zhang, C.; Kovalsky, P.; Waite, T. D. Comparison of Faradaic reactions in capacitive deionization (CDI) and membrane capacitive deionization (MCDI) water treatment processes. *Water Res.* **2017**, *120*, 229−237.

(18) Suss, M. E.; Presser, V. Water desalination with energy storage electrode materials. *Joule* **2018**, *2* (1), 10−15.

(19) Kim, T.; Gorski, C. A.; Logan, B. E. Low energy desalination using battery electrode deionization. *Environ. Sci. Technol. Lett.* **2017**, *4* (10), 444−449.

(20) Byles, B. W.; Cullen, D. A.; More, K. L.; Pomerantseva, E. Tunnel structured manganese oxide nanowires as redox active electrodes for hybrid capacitive deionization. *Nano Energy* **2018**, *44*, 476−488.

(21) Kim, S.; Yoon, H.; Shin, D.; Lee, J.; Yoon, J. Electrochemical selective ion separation in capacitive deionization with sodium manganese oxide. *J. Colloid Interface Sci.* **2017**, *506*, 644−648.

(22) Tang, W.; Liang, J.; He, D.; Gong, J.; Tang, L.; Liu, Z.; Wang, D.; Zeng, G. Various cell architectures of capacitive deionization: Recent advances and future trends. *Water Res.* **2019**, *150*, 225−251.
(23) Reale, E. R.; Shrivastava, A.; Smith, K. C. Effect of conductive additives on the transport properties of porous flow-through electrodes with insulative particles and their optimization for Faradaic deionization. *Water Res.* **2019**, *165*, 114995.
(24) Kim, T.; Gorski, C. A.; Logan, B. E. Ammonium removal from domestic wastewater using selective battery electrodes. *Environ. Sci. Technol. Lett.* **2018**, *5* (9), 578−583.
(25) Qin, M.; Deshmukh, A.; Epsztein, R.; Patel, S. K.; Owoseni, O. M.; Walker, W. S.; Elimelech, M. Comparison of energy consumption in desalination by capacitive deionization and reverse osmosis. *Desalination* **2019**, *455*, 100−114.
(26) Remillard, E. M.; Shocron, A. N.; Rahill, J.; Suss, M. E.; Vecitis, C. D. A direct comparison of flow-by and flow-through capacitive deionization. *Desalination* **2018**, *444*, 169−177.
(27) Avraham, E.; Bouhadana, Y.; Soffer, A.; Aurbach, D. Limitation of charge efficiency in capacitive deionization I. On the behavior of single activated carbon. *J. Electrochem. Soc.* **2009**, *156* (6), P95−P99.
(28) Suss, M. E.; Baumann, T. F.; Bourcier, W. L.; Spadaccini, C. M.; Rose, K. A.; Santiago, J. G.; Stadermann, M. Capacitive desalination with flow-through electrodes. *Energy Environ. Sci.* **2012**, *5* (11), 9511−9519.
(29) Avraham, E.; Noked, M.; Cohen, I.; Soffer, A.; Aurbach, D. The dependence of the desalination performance in capacitive deionization processes on the electrodes PZC. *J. Electrochem. Soc.* **2011**, *158* (12), P168−P173.
(30) Cohen, I.; Avraham, E.; Noked, M.; Soffer, A.; Aurbach, D. Enhanced charge efficiency in capacitive deionization Achieved by surface-treated electrodes and by means of a third electrode. *J. Phys. Chem. C* **2011**, *115* (40), 19856−19863.
(31) Zhang, C.; He, D.; Ma, J.; Tang, W.; Waite, T. D. Comparison of faradaic reactions in flow-through and flow-by capacitive deionization (CDI) systems. *Electrochim. Acta* **2019**, *299*, 727−735.
(32) Hawks, S. A.; Ramachandran, A.; Porada, S.; Campbell, P. G.; Suss, M. E.; Biesheuvel, P. M.; Santiago, J. G.; Stadermann, M. Performance metrics for the objective assessment of capacitive deionization systems. *Water Res.* **2019**, *152*, 126−137.
(33) Hemmatifar, A.; Ramachandran, A.; Liu, K.; Oyarzun, D. I.; Bazant, M. Z.; Santiago, J. G. Thermodynamics of Ion Separation by Electrosorption. *Environ. Sci. Technol.* **2018**, *52* (17), 10196−10204.
(34) Celik, E.; Liu, L.; Choi, H. Protein fouling behavior of carbon nanotube/polyethersulfone composite membranes during water filtration. *Water Res.* **2011**, *45* (16), 5287−5294.
(35) Geise, G. M.; Cassady, H. J.; Paul, D. R.; Logan, B. E.; Hickner, M. A. Specific ion effects on membrane potential and the permselectivity of ion exchange membranes. *Phys. Chem. Chem. Phys.* **2014**, *16* (39), 21673−21681.
(36) Le, X. T.; Bui, T. H.; Viel, P.; Berthelot, T.; Palacin, S. On the structure−properties relationship of the AMV anion exchange membrane. *J. Membr. Sci.* **2009**, *340* (1), 133−140.
(37) Geise, G. M.; Paul, D. R.; Freeman, B. D. Fundamental water and salt transport properties of polymeric materials. *Prog. Polym. Sci.* **2014**, *39* (1), 1−42.
(38) Wessells, C. D.; Peddada, S. V.; McDowell, M. T.; Huggins, R. A.; Cui, Y. The effect of insertion species on nanostructured open framework hexacyanoferrate battery electrodes. *J. Electrochem. Soc.* **2011**, *159* (2), A98−A103.
(39) Itaya, K.; Ataka, T.; Toshima, S. Spectroelectrochemistry and electrochemical preparation method of Prussian blue modified electrodes. *J. Am. Chem. Soc.* **1982**, *104* (18), 4767−4772.
(40) Wang, R. Y.; Shyam, B.; Stone, K. H.; Weker, J. N.; Pasta, M.; Lee, H. W.; Toney, M. F.; Cui, Y. Reversible multivalent (monovalent, divalent, trivalent) ion insertion in open framework materials. *Adv. Energy. Mater.* **2015**, *5* (12), 1401869.
(41) Scholz, F.; Dostal, A. The formal potentials of solid metal hexacyanometalates. *Angew. Chem., Int. Ed. Engl.* **1996**, *34* (23−24), 2685−2687.
(42) Wang, L.; Dykstra, J. E.; Lin, S. Energy Efficiency of Capacitive Deionization. *Environ. Sci. Technol.* **2019**, *53* (7), 3366−3378.
(43) Zhang, D.; Yan, T.; Shi, L.; Peng, Z.; Wen, X.; Zhang, J. Enhanced capacitive deionization performance of graphene/carbon nanotube composites. *J. Mater. Chem.* **2012**, *22* (29), 14696−14704.
(44) Wang, H.; Zhang, D.; Yan, T.; Wen, X.; Zhang, J.; Shi, L.; Zhong, Q. Three-dimensional macroporous graphene architectures as high performance electrodes for capacitive deionization. *J. Mater. Chem. A* **2013**, *1* (38), 11778−11789.
(45) Lin, S. Energy Efficiency of Desalination: Fundamental Insights from Intuitive Interpretation. *Environ. Sci. Technol.* **2019**, *54* (1), 76−84.

https://dx.doi.org/10.1021/acs.est.9b06843
Environ. Sci. Technol. 2020, 54, 3628−3635